Bioorganic Chemistry 87 (2019) 783–793

Contents lists available at ScienceDirect

Bioorganic Chemistry

journal homepage: www.elsevier.com/locate/bioorg

Furofuran lignans as a new series of antidiabetic agents exerting α-glucosidase inhibition and radical scarvenging: Semisynthesis, kinetic study and molecular modeling

Wisuttaya Worawalai[a], Titiruetai Doungwichitrkul[a], Warin Rangubpit[b], Panyakorn Taweechat[b], Pornthep Sompornpisut[b], Preecha Phuwapraisirisan[a,*]

[a] Center of Excellence in Natural Product, Department of Chemistry, Faculty of Science, Chulalongkorn University, Bangkok 10330, Thailand
[b] Center of Excellence in Computational Chemistry, Department of Chemistry, Faculty of Science, Chulalongkorn University, Bangkok 10330, Thailand

ARTICLE INFO

Keywords:
Diabetes mellitus
Glucosidase
Antioxidant
Furofuran lignan
Catechol

ABSTRACT

A new series of furofuran lignans containing catechol moiety were prepared from the reactions between lignans and a variety of phenolics. All 22 products obtained were evaluated against three different α-glucosidases (maltase, sucrase and Baker's yeast glucosidase) and DPPH radical. Of furofuran lignans evaluated, **β-14**, having two catechol moieties and one acetoxy group, was the most potent inhibitor against Baker's yeast, maltase, and sucrase with IC_{50} values of 5.3, 25.7, and 12.9 μM, respectively. Of interest, its inhibitory potency toward Baker's yeast was 28 times greater than standard drug, acarbose and its DPPH radical scavenging (SC_{50} 11.2 μM) was 130 times higher than commercial antioxidant BHT. Subsequent investigation on mechanism underlying the inhibitory effect of **β-14** revealed that it blocked Baker's yeast and sucrase functions by mixed-type inhibition while it exerted non-competitive inhibition toward maltase. Molecular dynamics simulation of the most potent furofuran lignans (**4**, **α-8b**, **α-14**, and **β-14**) with the homology rat intestinal maltase at the binding site revealed that the hydrogen bond interactions from catechol, acetoxy, and quinone moieties of furofuran lignans were the key interaction to bind tightly to α-glucosidase. The results indicated that **β-14** possessed promising antidiabetic activity through simultaneously inhibiting α-glucosidases and free radicals.

1. Introduction

Type 2 diabetes is a chronic disease in which there are high blood sugar levels over a prolonged period [1]. Uncontrolled hyperglycemia can impair many vital organs in the body, thus resulting in the development of microangiopathic complications such as nephropathy, retinopathy, and neuropathy [2]. One potential approach to alleviate diabetes is suppressing postprandial glucose concentration by inhibiting the α-glucosidase located in the brush border of the small intestine. Moreover, current evidences demonstrate that oxidative damage and the elevated generation of free radicals have been implicated in diabetic complications [3,4]. Thus, considerable efforts have been made to develop an antidiabetic drug that possesses both hypoglycemic and antioxidant properties [5].

In the course of our research for new antidiabetic agents having dual functions through inhibiting α-glucosidase and scavenging free radicals, we discovered arylalkanones from natural sources [6] together with quercitol derivatives via semisynthesis such as quercitylcinnamates [7], *N*-arylmethylaminoquercitols [8], and furofuran lignans containing one free hydroxy group [9]. Of natural derived antidiabetic agents synthesized in our laboratory, a furofuran lignan named sesamolin is considered as a versatile starter to facilely produce a variety of antidiabetic agents possessing dual functions in few steps. This approach was recently applied to synthesize a series of flavonolignans by the coupling between this lignan and various flavonoids [10]. Of flavonolignans synthesized, epicatechinosamin (**1**) encompassing catechol moiety (Fig. 1) displayed more potent inhibition against α-glucosidase and free radical than the other flavonolignans having no catechol moiety. This result suggests that the catechol moiety plays an important role in enhancing antidiabetic activity. A similar observation was also reported by Nakai [11] and Moazzami [12]. The catechol containing lignans **3** and **4** (Fig. 1) obtained via enzymatic oxidation of sesamin (**2**) showed dramatically enhanced radical scavenging over their starter **2**.

To further explore more potent antidiabetic agents and gain insight into the role of catechol moiety on inhibiting α-glucosidases and free

* Corresponding author.
E-mail address: peecha.p@chula.ac.th (P. Phuwapraisirisan).

https://doi.org/10.1016/j.bioorg.2019.03.077
Received 24 January 2019; Received in revised form 21 March 2019; Accepted 30 March 2019
Available online 05 April 2019
0045-2068/

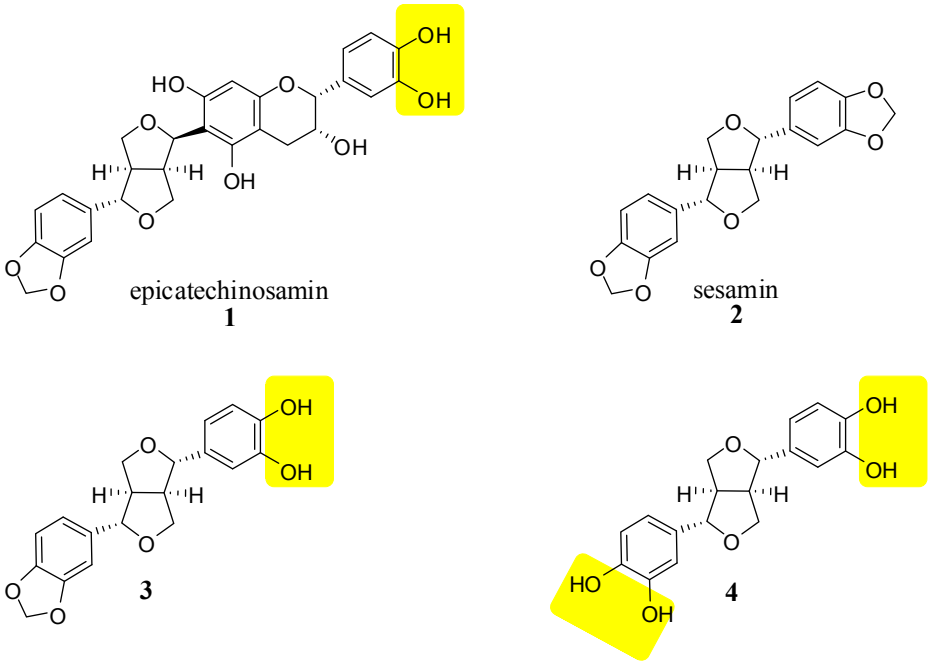

Fig. 1. Structures of lignans encompassing catechol moiety.

radicals, we herein demonstrate the efficient synthesis of a new series of furofuran lignans having multiphenolic and catechol moieties and report on α-glucosidase inhibitory effect and antioxidant activity of them. We also describe the mechanism underlying enzymatic inhibition and the molecular modeling of the most active furofuran lignans.

2. Results and discussion

2.1. Chemistry

Starting samin (**6**) was obtained from sesamolin, a naturally abundant lignan isolated from sesame (*Sesamum indicum*) seed oil, via acid hydrolysis (Scheme 1).

With the starter samin (**6**) in hand, furofuran lignans (**7a-7e**) were first synthesized via Friedel-Crafts reaction as showed in Scheme 2. Samin (**6**) reacted with a variety of electron-rich phenolics **a-e** in an acidic solution (Amberlyst-15, CH_3CN) at 70 °C to produce the diastereomeric furofuran lignans (**α-7a - α-7e** and **β-7a - β-7e**) in excellent yields. In this step, addition of a molecular sieve 4 Å to remove H_2O generated from the reaction was required.

Oxidative cleavage of the aromatic methylenedioxy moiety in furofuran lignans **7** was the critical step to afford the desired products containing catechol residue. The use of phosphorus pentachloride (PCl_5) in benzene yielded complex mixtures and starting material recovery. However, treatment of **7** with 3 equiv of lead tetraacetate ($Pb(OAc)_4$) [13] in toluene at 90 °C followed by acid hydrolysis in the presence of amberlyst-15 provide furofuran lignans **8** in a good yield (Scheme 2). The above result suggested that the reaction might proceed via displacement of a proton of the methylenedioxy moiety by an acetoxy group called orthoester type structure, which was then hydrolyzed by acid to obtain a catechol moiety [14]. Under this reaction, furofuran lignans (**7a-7c**) having one free phenolic hydroxy group were also oxidized by $Pb(OAc)_4$ to generate *para*-quinone moiety in **8**. Moreover, **α-9a** was obtained by only oxidation reaction. In contrast, treatment of **7d-7e**, containing two phenolic hydroxy groups, with $Pb(OAc)_4$ followed by acid hydrolysis affording the undesired product.

To solve this problem, protection of phenolic hydroxy group is required. Silylation of **α-7c** with *tert*-butyldimethylsilylchloride (TBDMSCl) gave **α-10c** in 51% yield. In addition, monosilylated products were observed in the case of furofuran lignans having two phenolic hydroxy groups (**7d** and **7e**). Subsequently, the methylenedioxy cleavage of **α-10c** was carried out under the similar conditions mentioned above using $Pb(OAc)_4$ followed by deprotection of TBS group concomitant with hydrolysis of the orthoester by using TBAF, affording **α-11c** in a fair yield. Unfortunately, the methylenedioxy cleavage of **10d** and **10e**, the lignans containing one free hydroxy group, failed to afford expected products.

Alternatively, furofuran lignans **14**, **3**, and **4** were also synthesized starting from sesamolin and sesamin, respectively (Scheme 3). Silylation of **12** gave **13** in excellent yields. The methylenedioxy cleavage and deprotection of **13** produced **14** in good yields. In addition, sesamin (**2**) was directly reacted with $Pb(OAc)_4$ and then hydrolyzed by amberlyst-15 to afford mono-catechol (**3**) and di-catechol (**4**) structures in excellent yields.

The relative configuration of the newly generated chiral center C-2 on the furan moiety of compounds **7a-7e**, and **12** was determined based on coupling constant analysis [9]. The α–isomer showed doublet of doublet (dd) for both H-4_{ax} and H-4_{eq} while the β–isomer displayed the dd pattern for H-4_{ax} but a unique doublet (d) for H-4_{eq} (Fig. 2). In addition, the structures of the synthesized compounds (**3**, **4**, **8**, **11**, and **14**) were characterized by ^1H NMR spectra which displayed no methylenedioxy singlet signal at δ ≈ 5.90 ppm (see Supplementary information).

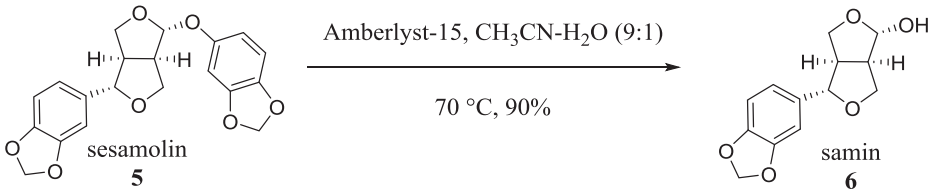

Scheme 1. Synthesis of samin (**6**).

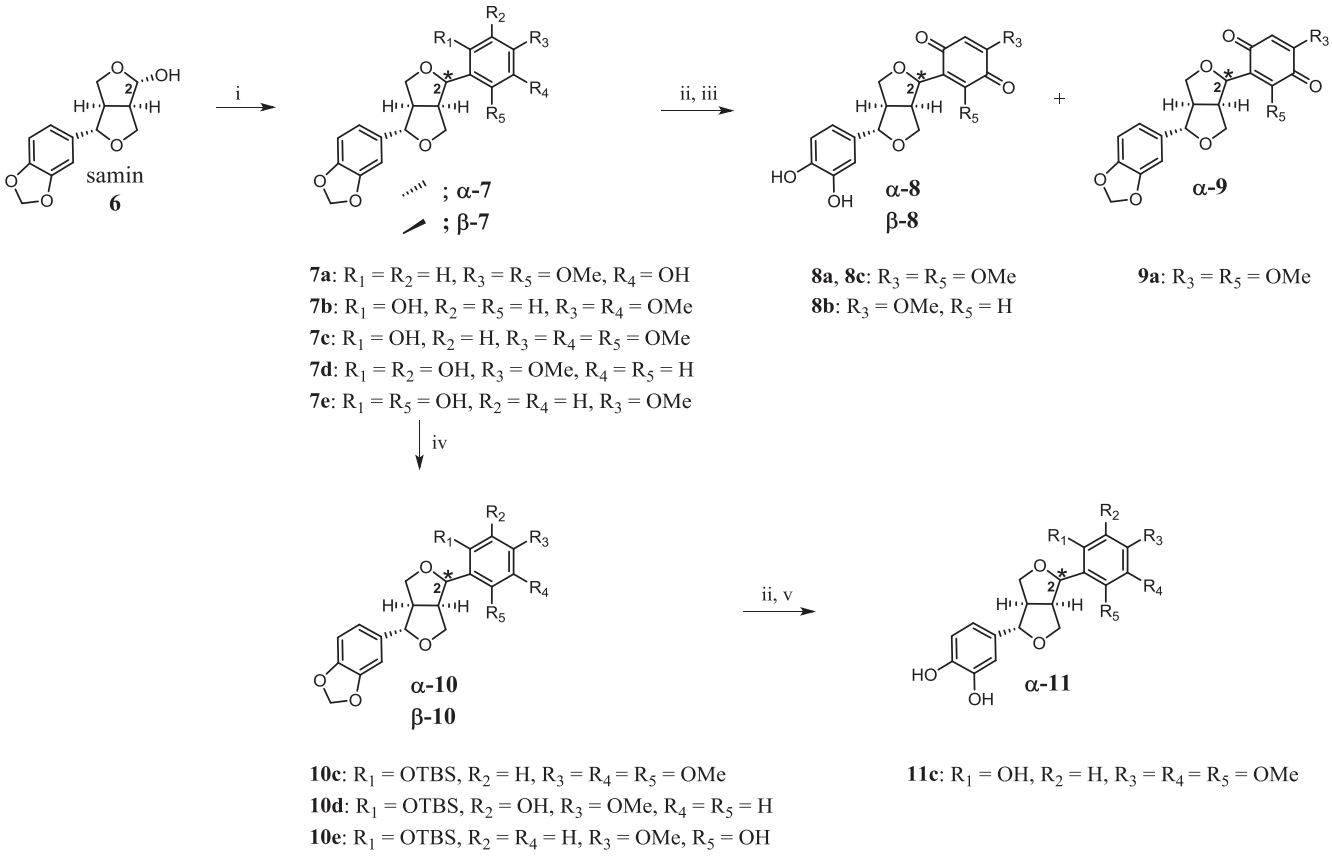

Scheme 2. Synthesis of furofuran lignans starting from samin. Reagents and conditions: (i) phenolics, amberlyst-15, CH_3CN, 4 Å MS, 70 °C, 8 h; (ii) $Pb(OAc)_4$, toluene, 90 °C, 2 h; (iii) amberlyst-15, CH_3CN-H_2O (8:2), 70 °C, 3 h; (iv) TBDMSCl, imidazole, DCM, rt, 12 h; (v) TBAF, THF, rt, 3 h.

2.2. α-Glucosidase inhibition

All furofuran lignans were evaluated for α-glucosidase inhibitory activity using enzymes from two different sources; baker's yeast (type I) and rat intestine (type II), and the results are shown in Table 1. As for Baker's yeast α–glucosidase, **7a**-**7c**, containing one phenolic hydroxy group, showed weak inhibition (IC_{50} 685.4-729.3 μM) whereas **7d** and **7e**, having two phenolic hydroxy groups, revealed higher inhibition (IC_{50} 25.4–56.4 μM). This result suggested that the inhibitory effect increased according to the number of phenolic hydroxy group. Interestingly, the inhibitory activity of furofuran lignans dramatically increased when encompassed catechol moiety (**3**, **4**, **8b**, **8c**, **α-11c**, and **14**). The furofuran lignans **8b** and **8c**, whose structures containing *para*-quinone and catechol moieties, displayed inhibitory effects in range of 14.6–23.4 μM, which is 30–50 times more potent than their furofuran starters (**7b** and **7c**). Similarly, **14**, having two catechol moieties, showed higher inhibition (IC_{50} 5.3–7.7 μM) than their starters **12** (IC_{50} 205.8–210.3 μM). These results were also observed in furofuran lignans **3** and **4**. Compound **4**, bearing two catechol moieties, exhibited stronger inhibition than **3** containing one catechol moiety, whereas

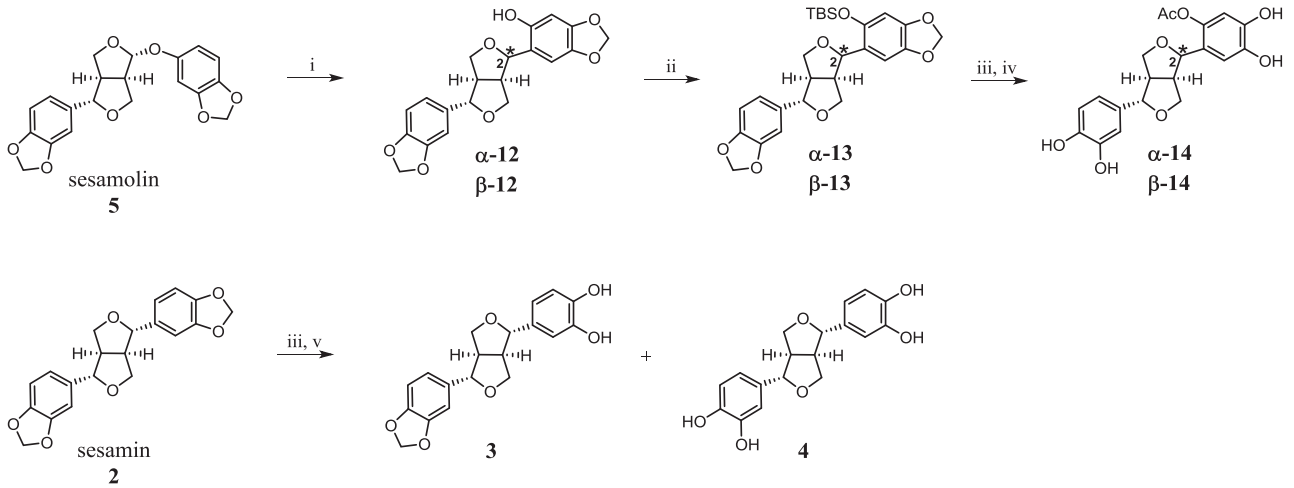

Scheme 3. Synthesis of furofuran lignans starting from sesamolin and sesamin. Reagents and conditions: (i) amberlyst-15, CH_3CN, 70 °C, 8 h; (ii) TBDMSCl, imidazole, DCM, rt, 12 h; (iii) $Pb(OAc)_4$, toluene, 90 °C, 2 h; (iv) TBAF, THF, rt, 3 h; (v) amberlyst-15, CH_3CN-H_2O (8:2), 70 °C, 3 h.

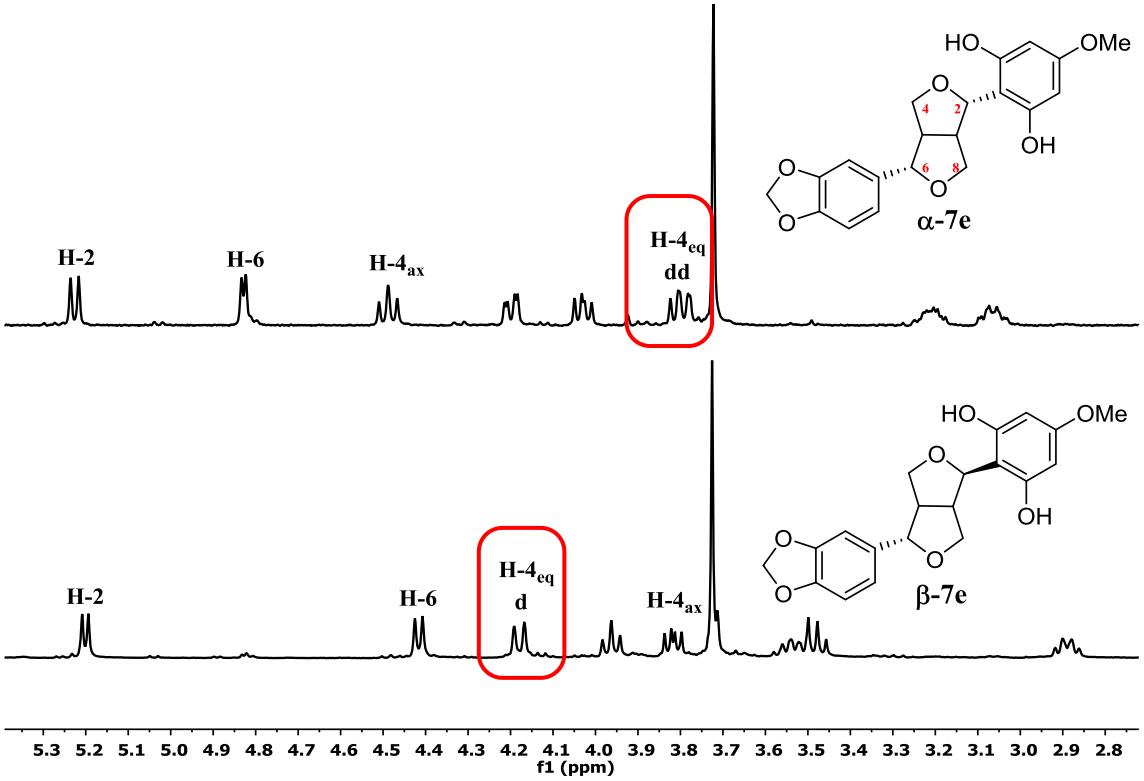

Fig. 2. ^{1}H NMR spectra of **α-7e** (top) and **β-7e** (bottom). For clarity, particular atoms are omitted.

Table 1
α-Glucosidase inhibitory effect and radical scavenging activity of furofuran lignans.

Compound	α-Glucosidase inhibitory effect (IC_{50}, μM)[a]			DPPH radical scavenging (SC_{50}, μM)[a]
	Baker's yeast	Maltase	Sucrase	
α-7a	700 ± 4.0	> 1000	> 1000	340 ± 5.7
β-7a	698 ± 3.8	> 1000	> 1000	171 ± 4.6
α-7b	729 ± 5.2	> 1000	> 1000	410 ± 5.4
β-7b	716 ± 3.7	> 1000	> 1000	220 ± 3.8
α-7c	692 ± 2.4	> 1000	> 1000	> 1000
β-7c	685 ± 2.1	> 1000	> 1000	> 1000
α-7d	32.2 ± 1.5	151 ± 0.9	180 ± 1.1	41.4 ± 1.1
β-7d	25.4 ± 1.4	110 ± 1.1	170 ± 1.7	39.0 ± 1.3
α-7e	56.4 ± 1.0	380 ± 3.5	340 ± 1.9	> 1000
β-7e	42.9 ± 1.7	260 ± 1.6	231 ± 2.4	> 1000
α-8a or **α-8c**	23.4 ± 1.2	96.5 ± 1.4	110 ± 1.0	82.6 ± 1.3
β-8a or **β-8c**	19.8 ± 1.9	63.3 ± 1.6	61.1 ± 1.8	79.5 ± 0.9
α-8b	15.9 ± 1.0	97.0 ± 1.2	46.6 ± 1.3	76.4 ± 1.4
β-8b	14.6 ± 0.7	47.0 ± 1.1	33.0 ± 0.2	67.8 ± 1.2
α-9a	> 1000	> 1000	> 1000	> 1000
α-11c	17.8 ± 1.8	174 ± 3.7	136 ± 3.2	72.6 ± 0.9
α-12	210 ± 1.2	> 1000	> 1000	650 ± 6.2
β-12	206 ± 1.1	> 1000	> 1000	420 ± 4.3
α-14	7.70 ± 0.6	38.8 ± 1.0	18.7 ± 0.3	12.3 ± 0.6
β-14	5.30 ± 0.6	25.7 ± 1.0	12.9 ± 0.4	11.2 ± 0.8
3	21.6 ± 1.4	170 ± 1.9	191 ± 3.7	90.3 ± 1.5
4	10.0 ± 1.0	42.6 ± 1.1	29.2 ± 1.2	14.7 ± 0.6
acarbose®	147 ± 0.5	1.40 ± 0.2	3.20 ± 0.4	ND[b]
BHT	ND	ND	ND	> 1000

[a] IC_{50} or SC_{50} values represent as mean ± SD of three determinations.
[b] Not determined.

their starter (sesamin) was not active. These results revealed that the presence of the catechol moiety might participate in chelation with enzymes, thus enhancing inhibitory activity [15]. Among furofuran lignans examined, **β-14**, bearing two catechol moieties and an acetoxy group, was the most potent inhibitor with an IC_{50} value of 5.3 μM, which is 28 times more active than the standard drug acarbose (IC_{50} 147.2 μM).

Further inspection of *para*-quinone moiety on inhibitory effect revealed that this moiety possibly worked together with catechol residue to inhibite the enzymes. Furofuran lignan **α-8a**, containing *para*-quinone and catechol moieties, showed the inhibition with an IC_{50} value of 23.4 μM, whereas **α-9a**, having no catechol moiety, was not active. In addition, **α-11c** (IC_{50} 17.8 μM) displayed the slightly higher inhibition than **α-8a** (IC_{50} 23.4 μM). This result suggested that phenolic hydroxy group might contribute major effect on the inhibition when compared with *para*-quinone moiety.

As for type II α–glucosidases (Table 1), most furofuran lignans inhibited sucrase more selectively than maltase. Generally, the inhibitory effect increased according to the number of phenolic hydroxy group, which was similar to the results observed in type I α–glucosidase. The remarkably increased inhibition was observed in a series of furofuran lignans having catechol moiety, when compared with their parents (weak inhibition). Of the synthesized lignans, **β-14** was the most potent inhibitor against maltase and sucrase with IC_{50} values of 25.7 and 12.9 μM, respectively. Moreover, *para*-quinone moiety also played an important role in inhibiting type II α-glucosidases. Lignan **α-8a**, bearing *para*-quinone residue, displayed the stronger inhibition against maltase and sucrase with IC_{50} values of 96.5 and 110.2 μM, respectively, when compared with **α-11c** having phenolic hydroxy group (IC_{50} 173.6 and 136.4 μM against maltase and sucrase, respectively). Noticeably, the β-isomer of all synthesized furofuran lignans exhibited higher inhibition than its epimer (α-isomer) in all bioactivities examined.

2.3. Evaluation of antioxidant activity

All synthesized furofuran lignans were also evaluated for antioxidation against DPPH radical (Table 1). This approach measures the hydrogen donating ability of the compound being studied. Furofuran lignans **7a**, **7b** and **12** (except **7c**, SC_{50} > 1000 μM), which have one free hydroxy group on phenolic moiety with an activating group such as

methoxy group at *ortho* or *para* position, showed weak DPPH radical scavenging activity in the range of 170.9–650.0 μM. In addition, furofuran lignans (**7d**, **8a-8c**, **α-11c**, and **3**), which contain one catechol moiety, displayed moderate DPPH radical scavenging activity in the range of 39.0–90.3 μM. However, **7e**, bearing two free hydroxy groups at meta position, did not reveal DPPH radical scavenging activity (SC_{50} > 1000 μM). These observations suggest that the presence of catechol moiety plays a critical role in trapping the radical. Remarkably, furofuran lignans **14** and **4**, containing two catechol moieties, revealed strong DPPH radical scavenging activity in the range of 11.2–14.7 μM, which is approximately 100 times more active than the standard BHT (SC_{50} 1560 μM).

2.4. Enzyme kinetic study

To evaluate the mechanisms of both type I and II α-glucosidase inhibitions of the furofuran lignans having catechol moiety, kinetic analysis was performed on the most potent inhibitors **4**, **α-8b**, **α-14**, and **β-14**. The Lineweaver-Burk plot of the active inhibitors (**4**, **α-8b**, **α-14**, and **β-14**) against Baker's yeast α-glucosidase displayed a series of straight lines; all of which intersected in the second quadrant (Fig. 3a for **β-14** and Figs. S1a, S2a and S3a for **4**, **α-8b**, and **α-14**, respectively). Kinetic analysis showed that V_{max} decreased with elevated K_m in the presence of increasing concentrations of the inhibitors. This behaviour suggested that **4**, **α-8b**, **α-14**, and **β-14** inhibited yeast α-glucosidase in a mixed-type manner comprising two different pathways, competitive and noncompetitive. The K_i and K'_i values were calculated directly by the secondary plots (Figs. S4–S7). All active compounds showed the K_i values less than the K_i' values (Table 2), indicating that all active compounds were predominantly bound to yeast α-glucosidase (EI) rather than forming ESI complex.

The inhibitory mechanisms of four active compounds against rat intestinal maltase and sucrase were also examined using the above methodology. The Lineweaver-Burk plots of **α-14** and **β-14** against maltase and sucrase (Fig. 3b and c for **β-14** and Figs. S3b and S3c for **α-14**) showed a series of straight lines; all of which intersected on the X-axis. Kinetic analysis showed that V_{max} decreased with unchanged K_m in the presence of increasing concentrations of inhibitors. This behaviour suggested that **α-14** and **β-14** were a non-competitive inhibitor against maltase and sucrase. The kinetic parameters of the active compounds are summarized in Table 2.

2.5. Cavities validation and molecular docking

We applied a homology model of the rat intestinal N-terminal domain of maltase-glucoamylase (rat-ntMGAM) which was reported in our previous study [16], and the active site of the model was inferred from the template structure (PDB: 3L4W). We further applied MetaPocket 2.0 (MPK2), a consensus method, to identify pocket for protein-ligand binding site prediction. The six metaPocket clusters probable binding sites of the rat intestinal maltase indicated using z-score from the biggest to smallest, 22.42, 8.48, 5.32, 2.62, 2.42, and 1.13, respectively as shown in Fig. S15.

The crude docking show the top three sites from the best three pockets. From the pocket area of site I and the docking results (Table 3) are in good agreement with previous study [15] as shown in Fig. S16. Therefore, systems were performed the molecular dynamics (MD) simulation.

2.6. Molecular dynamics simulation

The superimposition of the homology rat maltase-glucoamylase represented 91.6% similarities and 81.9% identities of Human Maltase-Glucoamylase (PDB:2QMJ) [17]. MD simulation of **α-8b**, **α-14**, **β-14**, and **4** complexes with rat maltase-glucoamylase approximately found the root mean square displacement (RMSD) of complexes compare to initial structure at 1.9 ± 0.05, 1.9 ± 0.08, 1.8 ± 0.07, and 2.0 ± 0.1 Å. Moreover, hydrogen bond analysis using VMD version 1.9 found the possibilities bonding around 1–4 hydrogen bond (Fig. S17) along trajectories calculations. The criteria for a hydrogen bond formation defined an atom between donor (D) and acceptor (A) atoms using cut-off distance is less than 3.0 Å and the angle of D-H-A is less than 20°. The interaction between the ligand and the enzyme formed between the hydroxy groups on aromatic ring of ligand or oxygen atom on furofuran core structure and the polar or charged residues of the enzyme at binding site I (Fig. 4). Surprisingly, the binding mode of two hydroxy groups on aromatic ring (catechol moiety) established the hydrogen bonds more than quinone part of **α-5b**. The detailed binding mode of **4** showed that two OH groups on aromatic ring (catechol moiety) established the strong hydrogen bonds with amino acid residue Arg580 whereas one OH group at para position from the other side formed a hydrogen bond to Asp837 (Fig. 4D, Table 4). In the case of **β-14**, two OH groups from catechol moiety formed hydrogen bonds with Arg343 and His705 while oxygen atom of furofuran core structure formed a hydrogen bond with Lys594 (Fig. 4C, Table 4). Furthermore, acetoxy group also created a hydrogen bond interaction with Lys836. As depicted in Fig. 4B, two OH groups from catechol moiety of **α-14** interacted with residues Arg580 and Phe595 while one OH group on aromatic ring at the meta position from the other side formed a hydrogen bond with Arg343. In addition, acetoxy group also interacted with residue Leu346. Compound **α-8b** showed the hydrogen bond interaction of oxygen atoms from *p*-quinone unit with amino acid residues Lys573 and Lys594. Moreover, OH groups from catechol moiety also formed hydrogen bonds with Arg580 (Fig. 4A, Table 4). Meanwhile, the complex was entering to equilibration state that each system was carry out free energy calculation of **α-8b**, **α-14**, **β-14**, and **4** complexes at −15.5, −14.7, −20.5, and −16.4 kcal/mol, respectively.

The binding free energy (ΔG_{bind}) for **α-8b**, **α-14**, **β-14** and **4** were −10.33, −11.17, −11.28 and −11.65 kcal/mol (Table 4), respectively. These results were consistent with the experimental results (K_i, Table 2) showing that compound **4** exhibit the highest binding affinity for rat maltase in pocket site I.

3. Conclusions

In summary, a new series of furofuran lignans containing catechol moiety were obtained by Friedel-Crafts reaction between samin and phenolics followed by the cleavage of the aromatic methylenedioxy moiety. This synthetic design was implemented in the hope that catechol part of the synthesized furofuran lignans would promote both α-glucosidase inhibition and antioxidant activity. Furofuran lignans **3**, **4**, **7d**, **8a-8c**, **α-11c**, and **14**, whose structures containing catechol moiety, showed remarkable inhibitory activity against rat intestinal maltase and sucrase as well as baker's yeast. Among them, **β-14**, having two catechol moieties and one acetoxy group, was the most potent inhibitor against α-glucosidases. In addition, furofuran lignans **8a-8c**, containing *para*-quinone and catechol moieties, displayed α-glucosidase inhibition more potent than **α-11c**, whose structure having one free hydroxy group instead of quinone moiety. This result suggests that *para*-quinone part might work together with catechol moiety to improve the activity. Further investigation of kinetic study indicated that the most active compounds **α-8b**, **α-14**, **β-14**, and **4** inhibited α-glucosidases (Baker's yeast, maltase, and sucrase) by mixed-type and non-competitive inhibition. This suggests that these inhibitors may bind to either the α-glucosidase or α-glucosidase-substrate complex at the binding site. Furthermore, the MD simulation of the most active compounds (**α-8b**, **α-14**, **β-14**, and **4**) towards maltase revealed that the hydrogen bonding from catechol, acetoxy, and quinone moieties was the key interaction to bind tightly to α-glucosidase. Moreover, DPPH radical scavenging activity revealed that furofuran lignans possessing catechol moiety also showed remarkable antioxidant property. Taken together, our results suggest that furofuran lignan **β-14** is promising candidate for the

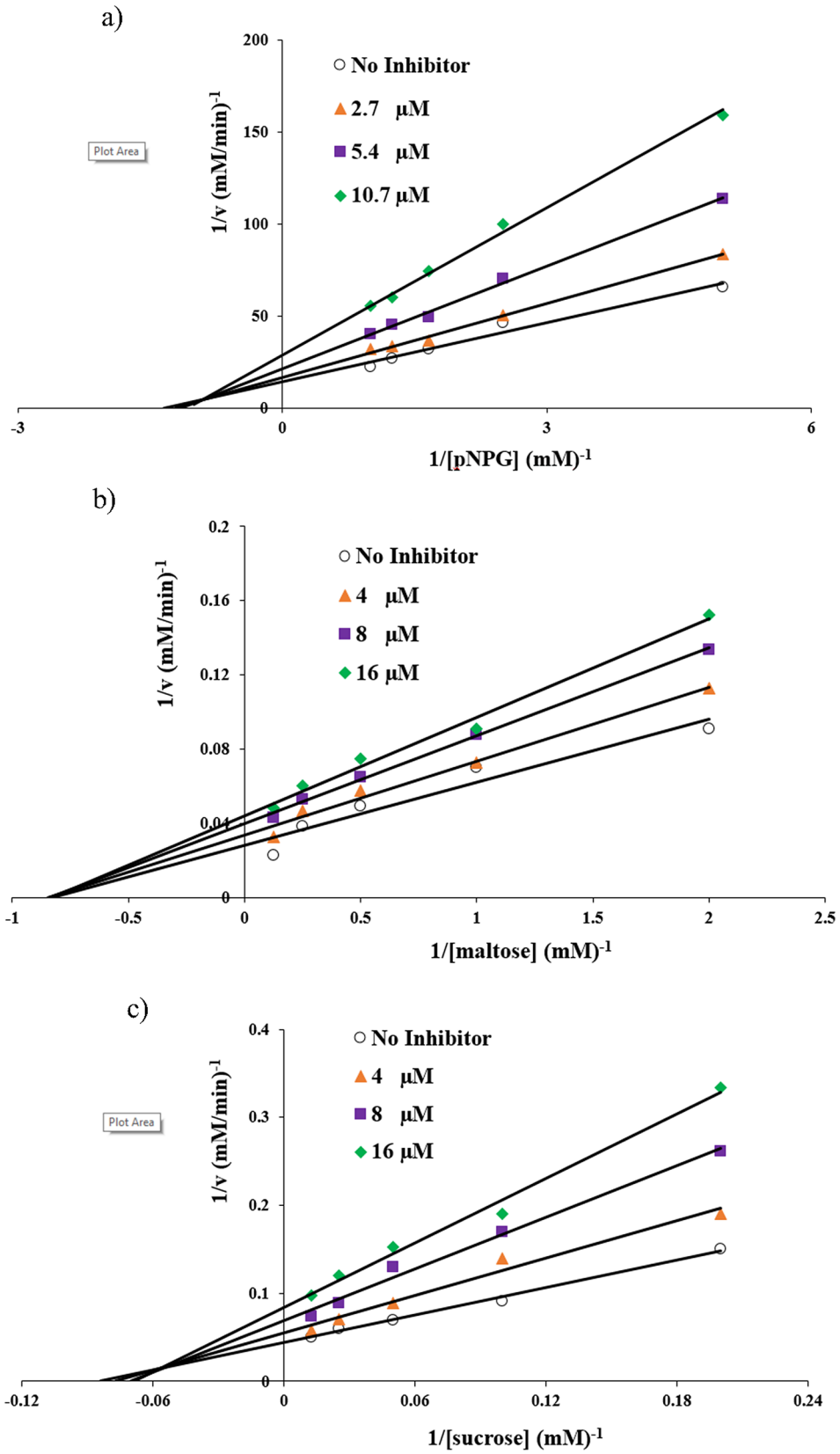

Fig. 3. Lineweaver-Burk plots for inhibitory activity of **β-14** against baker's yeast (a), maltase (b) and sucrase (c).

Table 2
Kinetic parameters of **α-8b**, **α-14**, **β-14**, and **4** on α-glucosidases.

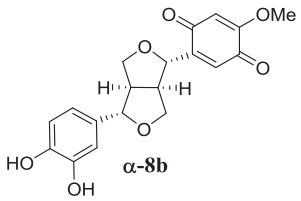

α-8b

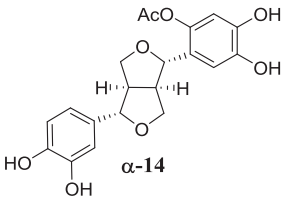

α-14

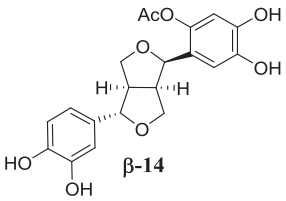

β-14

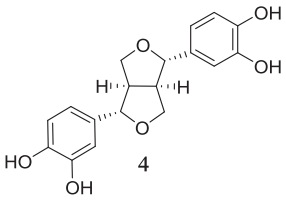

4

Compound	Baker's yeast			Maltase			Sucrase		
	K_i (μM)	K_i' (μM)	Inhibition type	K_i (μM)	K_i' (μM)	Inhibition type	K_i (μM)	K_i' (μM)	Inhibition type
α-8b	15.6 ± 0.5	59.7 ± 1.2	Mixed	67.8 ± 1.7	93.7 ± 1.1	Mixed	34.2 ± 0.9	62.7 ± 1.0	Mixed
α-14	10.1 ± 1.3	19.6 ± 1.3	Mixed	31.6 ± 1.1	–	Non-competitive	18.6 ± 0.7	–	Non-competitive
β-14	6.9 ± 0.8	10.4 ± 0.5	Mixed	28.4 ± 0.9	–	Non-competitive	11.6 ± 0.8	18.5 ± 1.0	Mixed
4	9.1 ± 0.6	16.5 ± 0.6	Mixed	19.9 ± 0.8	40.1 ± 1.5	Mixed	15.1 ± 0.7	39.9 ± 1.1	Mixed

Table 3
Binding glide scores of **α-8b**, **α-14**, **β-14**, and **4** on the homology rat intestinal maltase.

Evaluations	Compounds	Binding Sites		
		I	II	III
Blind Docking glide score (kcal/mol)	**α-8b**	−8.4	−8.9	−7.5
	α-14	−8.5	−8.5	−8.1
	β-14	−8.9	−8.5	−7.6
	4	−8.6	−9.0	−8.8
CDOCKER interaction (kcal/mol)	**α-8b**	−43.0	−43.7	−39.5
	α-14	−47.0	−47.4	−44.6
	β-14	−48.7	−50.3	−44.0
	4	−42.1	−46.2	−43.2

further development of diabetes treatment.

4. Experimental section

4.1. Chemistry

4.1.1. General procedure

All moisture-sensitive reactions were carried out under a nitrogen atmosphere. All solvents were distilled prior to use. High resolution electrospray ionisation mass spectra (HRESIMS) was recorded with a Bruker microTof spectrometer. ^{1}H and ^{13}C NMR spectra were recorded ($CDCl_3$ and CD_3OD as solvents) at 400 and 100 MHz, respectively, on a Varian Mercury$^+$ 400 NMR and a Bruker (Avance) 400 NMR spectrometer. Chemical shifts are reported in ppm downfield from TMS or solvent residue. Thin layer chromatography (TLC) was performed on pre-coated Merck silica gel 60 F_{254} plates (0.25 mm thick layer) and visualized by *p*-anisaldehyde reagent. Column chromatography was performed using Merck silica gel 60 (70–230 mesh) and Sephadex LH-20.

4.1.2. Hydrolysis of sesamolin (5)

To a solution of sesamolin (**5**, 0.27 mmol) in a mixture of acetonitrile/H_2O (9:1, 10 mL) was treated with acidic resin Amberlyst-15 (1 mg/0.005 mmol of **5**). After stirring at 70 °C for 8 h, the reaction mixture was evaporated to dryness and purified by silica gel column (50%EtOAc-hexane) to give samin **6** (60 mg, 90%) as a colorless oil.

4.1.3. General coupling reaction between samin and phenolics

To a solution of samin **6** (1 equiv) in acetonitrile (1.0 mL/0.1 mmol of **6**) was treated with phenolics (1.5–2 equiv), Amberlyst-15 (1 mg/0.005 mmol of **6**) and a 4 Å molecular sieve. After stirring at 70 °C for 8 h, the reaction mixture was evaporated to dryness and purified by silica gel column and Preparative TLC to afford furofuran lignans **7a-7e**.

4.1.3.1. α-7a. Yield: 36%, yellow oil; ^{1}H NMR (400 MHz, $CDCl_3$) δ 6.89–6.73 (m, 4H), 6.62 (d, J = 8.6 Hz, 1H), 5.94 (s, 2H), 5.05 (d, J = 4.0 Hz, 1H), 4.68 (d, J = 4.0 Hz, 1H), 4.31 (dd, J = 9.1, 7.3 Hz, 1H), 4.22 (dd, J = 9.1, 6.6 Hz, 1H), 4.01 (dd, J = 9.2, 4.7 Hz, 1H), 3.92 (d, J = 4.3 Hz, 4H), 3.89 (d, J = 7.1 Hz, 4H), 3.10–3.02 (m, 1H), 3.01–2.93 (m, 1H); ^{13}C NMR (100 MHz, $CDCl_3$) δ 148.1, 147.4, 144.6, 138.7, 135.4, 128.3, 119.6, 115.9, 108.3, 106.7, 105.9, 101.2, 85.6, 82.4, 73.1, 71.6, 60.6, 56.4, 54.8, 54.2; HRMS *m/z* 409.1260 [M + Na]$^+$ (calcd for $C_{21}H_{22}NaO_7$, 409.1263).

4.1.3.2. β-7a. Yield: 28%, yellow oil; ^{1}H NMR (400 MHz, $CDCl_3$) δ 7.02 (d, J = 8.5 Hz, 1H), 6.89–6.73 (m, 3H), 6.65 (d, J = 8.4 Hz, 1H), 5.95 (s, 2H), 4.95 (d, J = 5.9 Hz, 1H), 4.36 (d, J = 8.0 Hz, 1H), 4.09 (d, J = 9.4 Hz, 1H), 3.97–3.84 (m, 7H), 3.86–3.74 (m, 2H), 3.51–3.40 (m, 1H), 3.24 (t, J = 8.6 Hz, 1H), 2.86 (dd, J = 15.4, 7.2 Hz, 1H); ^{13}C NMR (100 MHz, $CDCl_3$) δ 148.1, 147.3, 147.2, 138.2, 135.5, 129.9, 124.6, 119.7, 116.8, 108.3, 106.8, 105.8, 101.2, 87.7, 78.7, 70.6, 69.9, 60.3, 56.4, 54.9, 49.2; HRMS *m/z* 409.1261 [M + Na]$^+$ (calcd for $C_{21}H_{22}NaO_7$, 409.1263).

4.1.3.3. α-7b. Yield: 42%, white powder; ^{1}H NMR (400 MHz, $CDCl_3$) δ 7.71 (brs, 1H, −OH), 6.84–6.79 (m, 3H), 6.54 (s, 1H), 6.49 (s, 1H), 5.96 (s, 2H), 4.82 (d, J = 8.0 Hz, 1H), 4.78 (d, J = 8.0 Hz, 1H), 4.36 (dd, J = 8.8, 7.2 Hz, 1H), 4.16 (dd, J = 9.6, 6.4 Hz, 1H), 3.92–3.86 (m, 2H), 3.84 (s, 3H, −OCH_3), 3.82 (s, 3H, −OCH_3), 3.21–3.14 (m, 2H); ^{13}C NMR (100 MHz, $CDCl_3$) δ 150.3, 150.1, 148.2, 147.4, 142.6, 134.8, 125.2, 119.5, 111.2, 108.4, 106.7, 102.1, 101.3, 86.7, 85.6, 72.6, 70.8, 57.2, 56.1, 53.6, 53.2; HRMS *m/z* 409.1286 [M + Na]$^+$ (calcd for $C_{21}H_{22}NaO_7$, 409.1263).

4.1.3.4. β-7b. Yield: 33%, white powder; ^{1}H NMR (400 MHz, $CDCl_3$) δ 8.05 (brs, 1H, −OH), 6.87–6.77 (m, 3H), 6.46 (s, 1H), 6.42 (s, 1H), 5.95 (s, 2H), 5.01 (d, J = 8.0 Hz, 1H), 4.44 (d, J = 6.8 Hz, 1H), 4.19 (d, J = 9.6 Hz, 1H), 3.98 (t, J = 8.8 Hz, 1H), 3.88 (m, 1H), 3.85 (s, 3H, −OCH_3), 3.80 (s, 3H, −OCH_3), 3.49 (dd, J = 8.4, 9.2 Hz, 1H), 3.40 (m, 1H), 2.91 (m, 1H); ^{13}C NMR (100 MHz, $CDCl_3$) δ 150.1, 149.8, 148.2, 147.5, 142.7, 134.8, 125.2, 119.8, 110.5, 108.4, 106.7, 101.9, 101.2, 87.7, 84.6, 71.9, 70.1, 57.0, 56.0, 53.7, 50.8; HRMS *m/z* 409.1275 [M + Na]$^+$ (calcd for $C_{21}H_{22}NaO_7$, 409.1263).

4.1.3.5. α-7c. Yield: 41%, colorless oil; ^{1}H NMR (400 MHz, $CDCl_3$) δ 8.58 (brs, 1H, −OH), 6.82–6.77 (m, 3H), 6.22 (s, 1H), 5.95 (s, 2H), 5.12 (d, J = 8.0 Hz, 1H), 4.83 (d, J = 8.0 Hz, 1H), 4.49 (dd, J = 8.4, 8.4 Hz, 1H), 4.13 (dd, J = 9.6, 2.8 Hz, 1H), 4.04 (dd, J = 9.2, 6.8 Hz, 1H), 3.90 (s, 3H, −OCH_3), 3.81 (s, 3H, −OCH_3), 3.80 (m, 1H), 3.79 (s, 3H,

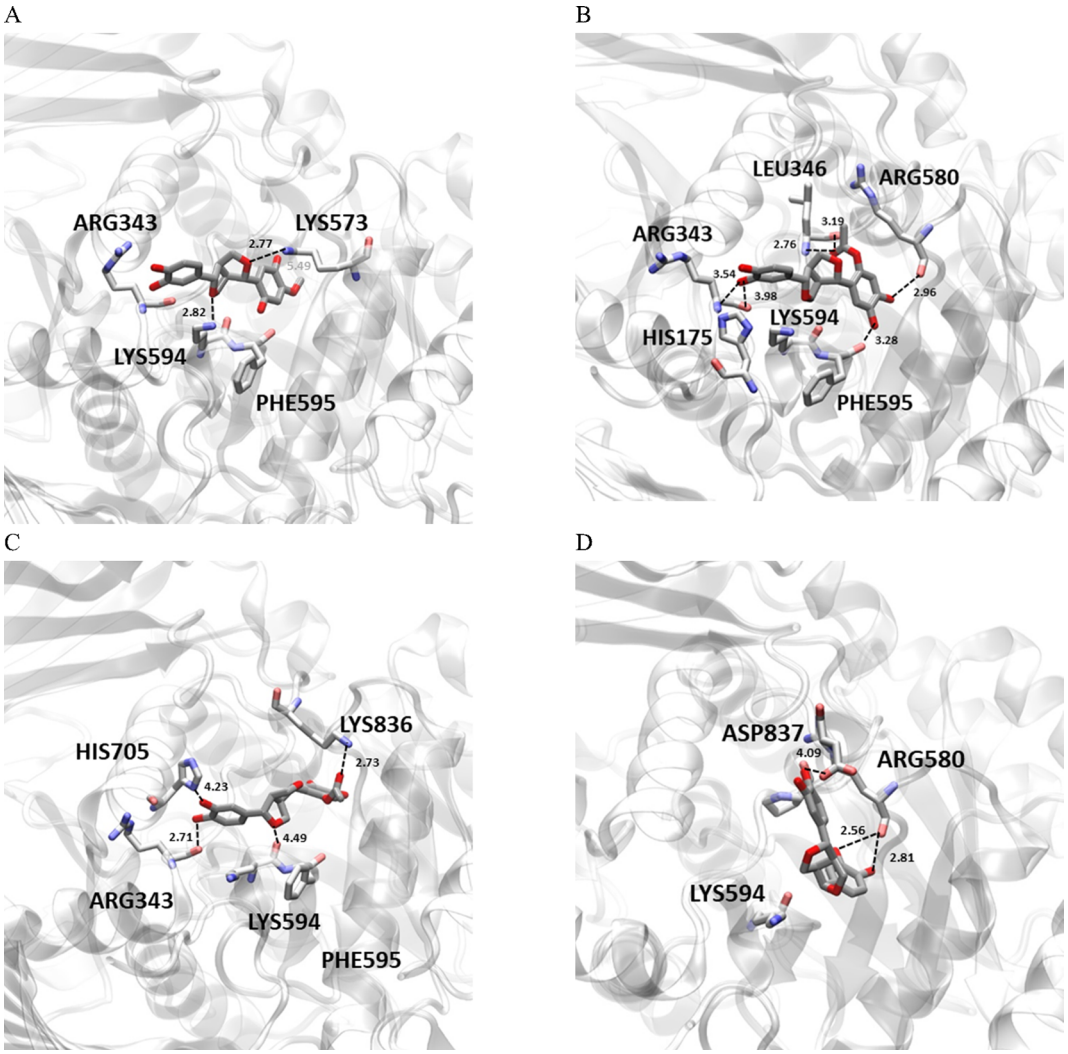

Fig. 4. Molecular dynamics analysis of four active lignans to the binding site 1 of homology rat intestinal maltase. Last snapshot of (A) **α-8b**, (B) **α-14**, (C) **β-14** and (D) **4** in 5 ns MD simulations.

Table 4
Molecular interaction results of the homology rat intestinal maltase at the binding site I with the active lignans **α-8b**, **α-14**, **β-14**, and **4**.

Compound	Binding free energy (ΔG_{bind} , kcal/mol)	H-bond interacting residue
α-8b	−10.33	LYS573, LYS594
α-14	−11.17	ARG343, ARG580, LEU346, PHE595
β-14	−11.28	ARG343, LYS594, LYS836, HIS705
4	−11.65	ASP837, ARG580

−OCH_3), 3.22 (m, 1H), 3.03 (m, 1H); ^{13}C NMR (100 MHz, $CDCl_3$) δ 153.9, 152.1, 150.9, 148.2, 147.3, 135.2, 134.7, 119.5, 109.1, 108.4, 106.8, 101.2, 97.0, 84.4, 84.2, 72.9, 70.8, 61.1, 60.9, 56.0, 54.7, 53.7; HRMS *m/z* 439.1366 $[M+Na]^+$ (calcd for $C_{22}H_{24}NaO_8$, 439.1369).

4.1.3.6. β-7c. Yield: 39%, colorless oil; ^{1}H NMR (400 MHz, $CDCl_3$) δ 8.87 (brs, 1H, −OH), 6.87 (s, 1H), 6.83–6.77 (m, 2H), 6.21 (s, 1H), 5.95 (s, 2H), 5.15 (d, J = 8.0 Hz, 1H), 4.40 (d, J = 4.0 Hz, 1H), 4.18 (d, J = 10.0 Hz, 1H), 3.92 (m, 1H), 3.90 (s, 3H, −OCH_3), 3.82 (s, 3H, −OCH_3), 3.79 (m, 1H), 3.78 (s, 3H, −OCH_3), 3.48–3.43 (m, 2H), 2.90 (m, 1H); ^{13}C NMR (100 MHz, $CDCl_3$) δ 153.8, 152.6, 150.2, 148.2, 147.5, 135.0, 134.8, 119.8, 108.3, 106.7, 105.7, 101.2, 96.8, 87.5, 82.0, 71.4, 70.3, 61.1, 60.9, 55.9, 53.8, 50.2; HRMS *m/z* 439.1366 $[M+Na]^+$ (calcd for $C_{22}H_{24}NaO_8$, 439.1369).

4.1.3.7. α-7d. Yield: 41%, brown oil; ^{1}H NMR (400 MHz, $CDCl_3$) δ 6.84 (s, 1H, H-6′), 6.77 (m, 2H, H-2′ and H-5′), 6.67 (d, J = 8.4 Hz, 1H, H-6″), 6.43 (d, J = 8.5 Hz, 1H, H-5″), 5.94 (s, 2H, H-7′), 4.97 (d, J = 5.4 Hz, 1H, H-2), 4.71 (d, J = 4.9 Hz, 1H, H-6), 4.25 (dt, J = 12.6, 8.4 Hz, 2H, H-4 and H-8), 3.94 (dd, J = 9.0, 3.8 Hz, 1H, H-8), 3.89 (m, 1H, H-4), 3.85 (s, 3H, -OMe), 3.18 (m, 1H, H-1), 3.05 (m, 1H, H-5); ^{13}C NMR (100 MHz, $CDCl_3$) δ 148.1, 147.2, 147.1, 142.5, 135.1, 133.6, 119.6, 119.5, 116.6, 108.3, 106.7, 103.0, 101.2, 85.6, 84.4, 72.0, 56.3, 54.1, 53.0.

4.1.3.8. β-7d. Yield: 21%, brown oil; ^{1}H NMR (400 MHz, $CDCl_3$) δ 6.86 (s, 1H, H-6′), 6.82–6.72 (m, 3H, H-2′, H-5′ and H-6″), 6.45 (d, J = 8.3 Hz, 1H, H-5″), 5.93 (s, 2H, H-7′), 5.00 (d, J = 5.8 Hz, 1H, H-2), 4.39 (d, J = 7.0 Hz, 1H, H-6), 4.12 (dd, J = 8.3, 5.4 Hz, 1H, H-4), 3.90 (m, 1H, H-8), 3.85 (s, 3H, -OMe), 3.81 (s, 1H, H-4), 3.45 (m, 1H,

H-1), 3.35 (m, 1H, H-8), 2.87 (dd, J = 15.3, 6.9 Hz, 1H, H-5); ^{13}C NMR (100 MHz, $CDCl_3$) δ 148.0, 147.3, 146.6, 142.0, 135.1, 133.1, 119.7, 118.9, 116.9, 108.2, 106.7, 103.1, 101.1, 87.6, 81.3, 71.2, 70.0, 56.2, 54.2, 49.5; HRMS m/z 395.1110 $[M+Na]^+$ (calcd for $C_{20}H_{20}NaO_7$, 395.1107).

4.1.3.9. α-7e. Yield: 5%, brown oil; ^{1}H NMR (400 MHz, $CDCl_3$) δ 6.98 (brs, 2H), 6.82 (s, 1H, H-6′), 6.77 (s, 2H, H-2′ and H-4′), 5.95 (d, J = 3.1 Hz, 2H, H-7′), 5.23 (d, J = 7.7 Hz, 1H, H-2), 4.83 (d, J = 3.9 Hz, 1H, H-6), 4.52–4.46 (m, 1H, H-4), 4.20 (dd, J = 9.4, 2.7 Hz, 1H, H-8), 4.03 (dd, J = 9.3, 6.7 Hz, 1H, H-8), 3.83–3.77 (m, 1H, H-4), 3.72 (s, 3H, -OMe), 3.25–3.17 (m, 1H, H-5), 3.10–3.02 (m, 1H, H-1); ^{13}C NMR (100 MHz, $CDCl_3$) δ 160.7, 156.0, 148.2, 147.3, 134.9, 119.5, 108.4, 106.8, 104.1, 101.2, 94.8, 84.4, 83.7, 72.9, 70.7, 55.4, 54.6, 53.7.

4.1.3.10. β-7e. Yield: 13%, brown oil; ^{1}H NMR (400 MHz, $CDCl_3$) δ 6.88–6.78 (m, 3H, H-2′, H-5′ and H-6′), 5.95 (s, 4H, H-7′, H-3″ and H-5″), 5.20 (d, J = 5.8 Hz, 1H, H-2), 4.42 (d, J = 7.1 Hz, 1H, H-6), 4.18 (d, J = 9.7 Hz, 1H, H-4), 3.96 (t, J = 8.3 Hz, 1H, H-8), 3.82 (dd, J = 9.7, 6.3 Hz, 1H, H-4), 3.73 (s, 3H, -OMe), 3.55 (m, 1H, H-1), 3.48 (m, 1H, H-8), 2.89 (m, 1H, H-5); ^{13}C NMR (100 MHz, $CDCl_3$) δ 160.7, 156.0, 148.2, 147.5, 134.8, 119.9, 108.3, 106.8, 101.2, 101.0, 94.5, 87.6, 81.7, 71.5, 70.3, 55.4, 53.6, 49.6; HRMS m/z 395.1111 $[M+Na]^+$ (calcd for $C_{20}H_{20}NaO_7$, 395.1107).

4.1.4. General protection of phenolic groups

To a solution of **α-7c**, **α-12**, and **β-12** (1 eq), imidazole (5 eq) in dichloromethane (DCM, 1.0 mL/0.1 mmol of starting material) was added *tert*-butyldimethylsilyl chloride (TBDMSCl) (5 eq). The mixture was stirred at room temperature for 12 h. The reaction mixture was washed with water and extracted with DCM (3 × 5 mL). The organic layer was washed with saturated aqueous NaCl, followed by dried over Na_2SO_4. After filtration and removal of the solvent under reduced pressure, the crude product was purified by silica gel column to obtain **α-10c**, **α-13**, and **β-13** in 51%, 70%, and 66% yield, respectively.

4.1.4.1. α-10c. Yield: 51%, pale yellow oil; ^{1}H NMR (400 MHz, $CDCl_3$) δ 6.86–6.77 (m, 3H), 6.16 (s, 1H), 5.95 (s, 2H), 5.18 (d, J = 7.0 Hz, 1H), 4.78 (d, J = 4.8 Hz, 1H), 4.35 (dd, J = 8.0, 8.0 Hz, 1H), 4.05 (m, 1H), 3.90 (s, 3H), 3.87–3.84 (m, 2H), 3.80 (s, 6H), 3.37 (m, 1H), 3.15 (m, 1H), 1.02 (s, 9H), 0.25 (s, 6H).

4.1.4.2. α-13. Yield: 70%, colorless oil; ^{1}H NMR (400 MHz, $CDCl_3$) δ 6.84–6.78 (m, 4H), 6.38 (s, 1H), 5.94 (s, 2H), 5.89 (d, J = 2.6 Hz, 2H), 5.06 (d, J = 3.6 Hz, 1H), 4.69 (d, J = 3.9 Hz, 1H), 4.29–4.23 (m, 2H), 3.93 (dd, J = 9.2, 3.8 Hz, 1H), 3.87 (dd, J = 9.2, 3.4 Hz, 1H), 2.99 (m, 2H), 1.01 (s, 9H), 0.24 (s, 3H), 0.24 (s, 3H).

4.1.4.3. β-13. Yield: 66%, colorless oil; ^{1}H NMR (400 MHz, $CDCl_3$) δ 7.05 (s, 1H), 6.88 (s, 1H), 6.84–6.76 (m, 2H), 6.37 (s, 1H), 5.94 (s, 2H), 5.91 (s, 2H), 4.88 (d, J = 6.2 Hz, 1H), 4.34 (d, J = 7.4 Hz, 1H), 4.08 (d, J = 9.4 Hz, 1H), 3.82–3.76 (m, 2H), 3.42 (m, 1H), 3.27 (m, 1H), 2.83 (m, 1H), 1.00 (s, 9H), 0.27 (s, 3H), 0.22 (s, 3H).

*4.1.5. General procedure for the preparation of compounds **8a–8c, 9a, 3** and **4***

A mixture of **7a–7c** and **2** (1 eq) and lead tetraacetate (3 eq) in toluene (1.0 mL/0.1 mmol of starting material) was stirred at 90 °C for 2 h. After being cooled to rt, the reaction mixture was diluted with toluene and filtered through a Celite pad. The filtrate was evaporated until dryness, washed with water and extracted with EtOAc (×3). The organic layer was dried with anhydrous sodium sulfate, and concentrated under reduced pressure to give a mixture of crude reaction. This mixture was then treated with amberlyst-15 (1 mg/0.005 mmol of starting material) in a mixture of MeCN-H_2O (8:2). After stirring at 70 °C for 3 h, the resulting mixture was evaporated to dryness and purified by silica gel column to give the target products **8a–8c**, **9a**, **3** and **4**.

*4.1.5.1. **α-8a** and **α-8c***. Yield: 81%, yellow oil; ^{1}H NMR (400 MHz, $CDCl_3$) δ 6.81–6.73 (m, 3H, H-2′, H-5′, and H-6′), 5.82 (s, 1H, H-3″), 5.15 (d, J = 5.6 Hz, 1H, H-2), 4.61 (d, J = 6.4 Hz, 1H, H-6), 4.26–4.17 (m, 2H, H-4 and H-8), 4.01 (s, 3H, H-8″), 3.89–3.83 (m, 2H, H-4 and H-8), 3.79 (s, 3H, H-7″), 3.23 (m, 1H, H-1), 3.12 (m, 1H, H-5); ^{13}C NMR (100 MHz, $CDCl_3$) δ 187.0, 178.6, 157.4, 155.4, 144.1, 143.9, 133.6, 130.3, 118.8, 115.5, 113.6, 107.6, 85.5, 78.3, 72.8, 72.7, 61.9, 56.6, 55.5, 52.0; HRESIMS m/z 411.1067 $[M+Na]^+$ (calcd for $C_{20}H_{20}NaO_8$, 411.1056).

*4.1.5.2. **β-8a** and **β-8c***. Yield: 70%, yellow oil; ^{1}H NMR (400 MHz, $CDCl_3$) δ 6.79–6.73 (m, 3H), 5.83 (s, 1H), 4.90 (d, J = 6.6 Hz, 1H), 4.40 (d, J = 7.4 Hz, 1H), 4.03–4.01 (m, 2H), 3.99 (s, 3H), 3.80 (s, 3H), 3.70 (dd, J = 9.4, 6.0 Hz, 1H), 3.53 (dd, J = 8.3, 8.3 Hz, 1H), 3.36 (m, 1H), 2.85 (m, 1H); ^{13}C NMR (100 MHz, $CDCl_3$) δ 187.2, 178.4, 157.6, 155.7, 144.1, 144.1, 133.1, 128.7, 119.0, 115.5, 113.7, 107.4, 86.7, 77.9, 70.8, 70.0, 62.2, 56.7, 54.3, 49.9; HRESIMS m/z 411.1067 $[M+Na]^+$ (calcd for $C_{20}H_{20}NaO_8$, 411.1056).

4.1.5.3. α-8b. Yield: 68%, yellow oil; ^{1}H NMR (400 MHz, CD_3OD) δ 6.79 (d, J = 2.0 Hz, 1H, H-2′), 6.73 (d, J = 8.1 Hz, 1H, H-5′), 6.67 (dd, J = 8.1, 2.0 Hz, 1H, H-6′), 6.63 (s, 1H, H-6″), 6.02 (s, 1H, H-3″), 4.77 (d, J = 2.8 Hz, 1H, H-2), 4.56 (d, J = 5.4 Hz, 1H, H-6), 4.29 (dd, J = 9.3, 6.7 Hz, 1H, H-8), 4.14 (dd, J = 9.1, 5.8 Hz, 1H, H-4), 4.05 (dd, J = 9.3, 4.0 Hz, 1H, H-8), 3.89 (dd, J = 9.1, 3.2 Hz, 1H, H-4), 3.82 (s, 3H, H-7″), 2.98–2.95 (m, 2H, H-1 and H-5); ^{13}C NMR (100 MHz, CD_3OD) δ 189.0, 183.5, 160.5, 150.6, 146.5, 146.1, 133.6, 128.6, 118.9, 116.3, 114.5, 108.7, 86.7, 82.6, 74.2, 72.6, 57.0, 55.2, 54.3; HRESIMS m/z 381.0949 $[M+Na]^+$ (calcd for $C_{19}H_{18}NaO_7$, 381.0950).

4.1.5.4. β-8b. Yield: 64%, yellow oil; ^{1}H NMR (400 MHz, CD_3OD) δ 6.80 (d, J = 1.9 Hz, 1H, H-2′), 6.78 (s, 1H, H-6″), 6.73 (d, J = 8.1 Hz, 1H, H-5′), 6.68 (dd, J = 8.1, 2.0 Hz, 1H, H-6′), 6.03 (s, 1H, H-3″), 4.70 (d, J = 6.7 Hz, 1H, H-2), 4.26 (d, J = 7.4 Hz, 1H, H-6), 4.04 (d, J = 9.4 Hz, 1H, H-4), 3.87 (m, 1H, H-8), 3.84 (s, 3H, H-7″), 3.81 (m, 1H, H-4), 3.49 (m, 1H, H-1), 3.28 (m, 1H, H-8), 2.92 (m, 1H, H-5); ^{13}C NMR (100 MHz, CD_3OD) δ 188.2, 183.0, 160.6, 148.1, 146.5, 146.3, 133.5, 131.1, 119.0, 116.2, 114.5, 108.4, 89.0, 78.6, 71.5, 70.3, 57.0, 55.8, 50.3; HRESIMS m/z 381.0949 $[M+Na]^+$ (calcd for $C_{19}H_{18}NaO_7$, 381.0950).

4.1.5.5. α-9a. Yield: 20%, yellow oil; ^{1}H NMR (400 MHz, $CDCl_3$) δ 6.84 (d, J = 0.8 Hz, 1H, H-6′), 6.79–6.75 (m, 2H, H-2′ and H-5′), 5.93 (s, 2H, H-7′), 5.82 (s, 1H, H-5″), 5.13 (d, J = 5.5 Hz, 1H, H-2), 4.62 (d, J = 6.6 Hz, 1H, H-6), 4.21 (m, 2H, H-4 and H-8), 4.00 (s, 3H, -OMe), 3.87–3.82 (m, 2H, H-4 and H-8), 3.78 (s, 3H, -OMe), 3.24–3.19 (m, 1H, H-1), 3.10–3.05 (m, 1H, H-5); ^{13}C NMR (100 MHz, $CDCl_3$) δ 186.8, 178.6, 157.3, 155.3, 148.1, 147.3, 135.3, 130.6, 119.6, 108.3, 107.6, 107.5, 106.6, 101.2, 85.5, 78.2, 72.9, 72.6, 61.8, 56.6, 55.9, 52.1; HRMS m/z 423.1057 $[M+Na]^+$ (calcd for $C_{21}H_{20}NaO_8$, 423.1056).

4.1.5.6. 3. Yield: 15%, brown oil; ^{1}H NMR (400 MHz, CD_3OD) δ 7.26–7.12 (m, 5H), 7.08 (dd, J = 8.1, 1.7 Hz, 1H), 6.31 (s, 2H), 5.25 (brs, 2H), 5.07 (d, J = 4.7 Hz, 1H), 5.03 (d, J = 4.6 Hz, 1H), 4.59 (dd, J = 6.4, 2.6 Hz, 1H), 4.23–4.18 (m, 2H), 3.72–3.70 (m, 1H), 3.46 (t, J = 11.0 Hz, 2H). The data were consistent with previous report [13].

4.1.5.7. 4. Yield: 71%, dark brown oil; ^{1}H NMR (400 MHz, CD_3OD) δ 6.82–6.68 (m, 6H), 4.63 (d, J = 4.3, 2H), 4.21 (dd, J = 9.0, 7.1 Hz, 2H), 3.80 (dd, J = 9.0, 3.5 Hz, 2H), 3.07 (m, 2H); ^{13}C NMR (100 MHz, CD_3OD) δ 145.0, 144.5, 132.4, 116.9, 115.2, 113.5. 84.9, 70.7, 53.5. The data were consistent with previous report [13].

*4.1.6. General procedure for the preparation of compounds **α-11c** and **14***

A mixture of **α-10c** and **13** (1 eq) and lead tetraacetate (5 eq) in toluene (1.0 mL/0.1 mmol of starting material) was stirred at 90 °C for 2 h. After being cooled to rt, the reaction mixture was diluted with toluene and filtered through a Celite pad. The filtrate was evaporated until dryness, washed with water and extracted with EtOAc (×3). The organic layer was dried with anhydrous sodium sulfate, and concentrated under reduced pressure to give a mixture of crude reaction. This mixture was then treated with tetrabutylammonium fluoride hydrate (TBAF, 5 eq) in THF (1.0 mL/0.1 mmol of starting material) at rt for 3 h. After being quenched with water, the resulting mixture was extracted with EtOAc (×3). The extracts were washed with saturated aqueous NaCl, followed by dried over Na_2SO_4. After filtration and removal of the solvent under reduced pressure, the crude product was purified by Sephadex LH-20 column (100% MeOH) to afford **α-11c** and **14**.

4.1.6.1. α-11c. Yield: 70%, brown oil; ^{1}H NMR (400 MHz, $CDCl_3$) δ 8.60 (s, 1H, −OH), 6.87–6.81 (m, 2H, H-5′ and H-6′), 6.73 (s, 1H, H-2′), 6.22 (s, 1H, H-3″), 5.60 (brs, 1H, −OH), 5.46 (brs, 1H, −OH), 5.11 (d, J = 7.4 Hz, 1H, H-2), 4.82 (d, J = 3.3 Hz, 1H, H-6), 4.49 (t, J = 8.5 Hz, 1H, H-4), 4.12 (d, J = 7.5 Hz, 1H, H-8), 4.02 (m, 1H, H-8), 3.90 (s, 3H, -OMe), 3.81 (s, 3H, -OMe), 3.79 (m, 1H, H-4), 3.78 (s, 3H, -OMe), 3.23 (m, 1H, H-5), 3.02 (m, 1H, H-1); ^{13}C NMR (100 MHz, $CDCl_3$) δ 153.9, 152.1, 143.9, 143.3, 135.4, 133.8, 125.2, 118.9, 115.5, 113.5, 109.2, 97.0, 84.4, 83.9, 73.0, 70.7, 61.1, 61.0, 56.0, 54.7, 53.4.

4.1.6.2. α-14. Yield: 36%, dark brown oil; ^{1}H NMR (400 MHz, CD_3OD) δ 6.85 (s, 1H, H-6″), 6.80 (s, 1H, H-6′), 6.75 (d, J = 8.1 Hz, 1H, H-5′), 6.68 (d, J = 7.6 Hz, 1H, H-2′), 6.52 (s, 1H, H-3″), 4.75 (d, J = 4.3 Hz, 1H, H-2), 4.61 (d, J = 4.3 Hz, 1H, H-6), 4.20 (dd, J = 16.1, 9.4 Hz, 2H, H-4 and H-8), 3.81 (dd, J = 8.8, 3.2 Hz, 2H, H-4 and H-8), 3.05 (s, 2H, H-1 and H-5), 2.27 (s, 3H, H-8″); ^{13}C NMR (100 MHz, CD_3OD) δ 171.59, 146.42, 146.22, 146.07, 144.49, 141.90, 133.77, 125.36, 118.90, 116.28, 114.48, 113.75, 111.03, 87.07, 82.89, 73.08, 72.79, 55.36, 55.03, 54.77, 20.83; HRMS m/z 411.1058 $[M+Na]^+$ (calcd for $C_{20}H_{20}NaO_8$, 411.1056).

4.1.6.3. β-14. Yield: 45%, yellow oil; ^{1}H NMR (400 MHz, CD_3OD) δ 7.02 (s, 1H, H-6″), 6.80 (s, 1H, H-2′), 6.74 (d, J = 8.3 Hz, 1H, H-5′), 6.69 (d, J = 7.9 Hz, 1H, H-6′), 6.50 (s, 1H, H-3″), 4.75 (d, J = 5.3 Hz, 1H, H-2), 4.30 (d, J = 7.3 Hz, 1H, H-6), 4.03 (d, J = 9.3 Hz, 1H, H-4), 3.78–3.74 (m, 2H, H-4 and H-8), 3.25–3.23 (m, 2H, H-1 and H-8), 2.88 (m, 1H, H-5), 2.28 (s, 3H, H-8″); ^{13}C NMR (100 MHz, CD_3OD) δ 171.6, 146.4, 146.1, 145.8, 144.1, 140.9, 133.7, 122.6, 119.0, 116.3, 114.5, 114.4, 110.7, 89.1, 79.2, 71.4, 70.3, 55.6, 50.2, 20.8; HRESIMS m/z 411.1053 $[M+Na]^+$ (calcd for $C_{20}H_{20}NaO_8$, 411.1056).

4.2. α-Glucosidase inhibitory activity

α-Glucosidase inhibitory activity against baker's yeast was determined according to our previous report [7]. The synthesized compounds (1 mg/mL in DMSO, 10 μL) were pre-incubated with 40 μL of α-glucosidase (0.1 U/mL in 0.1 M phosphate buffer, pH 6.9) at 37 °C for 10 min. The mixture was added with 50 μL of substrate solution (1 mM *p*-nitrophenyl-α-D-glucopyranoside, pNPG) and incubated for 20 min. The resulting mixture was quenched by adding 100 μL of 1 M Na_2CO_3. *p*-Nitrophenoxide ion liberated from the enzymatic reaction was monitored at 405 nm by Bio-Rad 3550 microplate reader. The percentage inhibitionwas calculated by $[(A_0 - A_1)/A_0] \times 100$, where A_1 and A_0 are the absorbance with and without the sample, respectively. The IC_{50} value was deduced from a plot of percentage inhibition versus sample concentration and acarbose was used as a positive control.

α-Glucosidase inhibitory activity against rat intestinal maltase and sucrase was determined according to our previous report [6]. The crude enzyme solution prepared from rat intestinal acetone powder (Sigma, St. Louis) was used as a source of maltase and sucrase. Rat intestinal acetone powder (1 g) was homogenized in 30 mL of 0.9% NaCl solution. After centrifugation (12,000 g × 30 min), the aliquot was subjected to assay. The synthesized compounds (1 mg/mL in DMSO, 10 μL) were added with 30 μL of the 0.1 M phosphate buffer (pH 6.9), 20 μL of the substrate solution (maltose: 2 mM; sucrose: 20 mM) in 0.1 M phosphate buffer, 80 μL of glucose assay kit (SU-GLLQ2, Human), and 20 μL of the crude enzyme solution. The reaction mixture was then incubated at 37 °C for 10 min (for maltose) and 40 min (for sucrose). Enzymatic activity was quantified by measuring the absorbance of quinoneimine formed (500 nm) using Bio-Rad 3550 microplate reader. The percentage inhibition was calculated using the above expression.

4.3. Kinetic study of α-glucosidase inhibition

For kinetic analysis of the active compound, α-glucosidases and active compounds were incubated with increasing concentrations of pNPG (0.2–1 mM), maltose (0.5–8 mM), and sucrose (5–80 mM). The type of inhibition was determined by the Lineweaver-Burk plot. For calculation of K_i and K_i' values, slope and intercept from the Lineweaver-Burk plot were replotted vs. [I], which provided the secondary plot.

4.4. DPPH radical scavenging

Radical scavenging activity was validated using DPPH colorimetric method. Briefly, The synthesized compounds (20 μL) were added to 0.1 mM methanolic solution of DPPH (100 μL). The mixture was kept dark at room temperature in an incubator shaker for 15 min. The absorbance of the resulting solution was measured at 517 nm with a 96-well microplate reader. The percentage inhibition was calculated by $[(A_0\text{-}A_1)/A_0] \times 100$, where A_0 is the absorbance without the sample, and A_1 is the absorbance with the sample. The SC_{50} value was deduced from a plot of percentage inhibition versus sample concentration. Butylated hydroxytoluene (BHT) was used as the standard control and the experiment was performed in triplicate.

4.5. Modeling studies

4.5.1. Pocket verification and docking methods

A homology model of the rat intestinal N-terminal domain of maltase-glucoamylase (rat-ntMGAM) used in this experiment came from our previous study [16]. Crude protein pocket or cavity using Fpocket [18], the detection algorithm based on Voronoi tessellation [19], and Metapocket [20], the protocol consensus among eight different method, seek the biggest cavities. Additionally, the Achilles Blind docking server [21] use to validate overlap area with seeking pocket programs, which explore the ligand template match orientations and cavities to identify putative ligand binding sites. However, each compound was individually docked into the best candidate cavity of maltase-glucoamylase (α-glucosidases) using the CDOCKER [22] implemented in Discovery Studio 3.0 (Accelrys Inc). According to the docking procedure using the CHARMM force field that is simulated annealing search algorithm and energy minimization [23]. The ~9 Å radius sphere around ligand was defined to docking site. The docked 100 random orientations were chosen the lowest CDOCKER interaction energy.

4.5.2. Molecular dynamics simulation

MD simulations were carried out under the periodic boundary condition (PBC) using the NAMD program package [24]. The CHRAMM 36 [25–28] force field and CHARMM General Force Field (CGENFF) were used to treat protein and ligand, respectively. Each complex was embedded in a three dimensional box of 130 × 130 × 130 Å^3 consisting of ~10 000 (9260) TIP3P [29] water molecules. After neutralization by Na^+ and Cl^- ions, the all-atom simulation box model consists of ~200 000 atoms (204 675). In addition, the solvent was

energetically relaxed by 5000 steps of energy minimization and 50 000 steps of solute-restrained MD simulations. Subsequently, every 100 000 steps were applied to system with whole protein-ligand, protein backbone-ligand, and ligand, respectively, restrained. The particle mesh Ewald (PME) summation method [30,31] was used to calculate the long-range electrostatic interactions. System was heated from 0 to 298 K with the NPT ensemble using the Nosé-Hoover Langevin piston pressure control [32]. For each system, unrestrained MD simulations were conducted for 5 ns.

Acknowledgements

This project was financially supported by the Thailand Research Fund (RSA5880027) and Faculty of Science, Chulalongkorn University (Sci-Super IV_61_003). W.W. and W.R. are grateful to the Graduate School of Chulalongkorn University for a Postdoctoral Fellowship (Ratchadaphisek Sompot Fund) and a PhD Scholarship (Dusadi Phipat), respectively. The Centers of Excellent in Natural Products (CENP) and Computational Chemistry (CECC) were subsidized by Chulalongkorn University.

Appendix A. Supplementary material

Supplementary data to this article can be found online at https://doi.org/10.1016/j.bioorg.2019.03.077.

References

[1] C.Y. Cai, L. Rao, Y. Rao, J.X. Guo, Z.Z. Xiao, J.Y. Cao, Z.S. Huang, B. Wang, Analogues of xanthones–chalcones and bis-chalcones as α-glucosidase inhibitors and anti-diabetes candidates, Eur. J. Med. Chem. 130 (2017) 51–59.
[2] G. Wang, Z. Peng, J. Wang, X. Li, J. Li, Synthesis, in vitro evaluation and molecular docking studies of novel triazine-triazole derivatives as potential α-glucosidase inhibitors, Eur. J. Med. Chem. 125 (2017) 423–429.
[3] M. Brownlee, Biochemistry and molecular cell biology of diabetic complications, Nature 414 (2001) 813–820.
[4] A.C. Maritim, R.A. Sanders, J.B. Watkins III, Diabetes, oxidative stress, and antioxidants: a review, J. Biochem. Mol. Toxicol. 17 (2003) 24–38.
[5] E. Ladopoulou, A.N. Matralis, A.P. Kourounakis, New multifunctional di-*tert*-butylphenoloctahydro(pyrido/benz)oxazine derivatives with antioxidant, antihyperlipidemic, and antidiabetic action, J. Med. Chem. 56 (2013) 3330–3338.
[6] R. Ramadhan, P. Phuwapraisirisan, New arylalkanones from *Horsfieldia macrobotrys*, effective antidiabetic agents concomitantly inhibiting α-glucosidase and free radicals, Bioorg. Med. Chem. Lett. 25 (2015) 4529–4533.
[7] E. Rattanangkool, P. Kittikhunnatham, T. Damsud, S. Wacharasindhu, P. Phuwapraisirisan, Quercitylcinnamates, a new series of antidiabetic bioconjugates possessing α-glucosidase inhibition and antioxidant, Eur. J. Med. Chem. 66 (2013) 296–304.
[8] W. Worawalai, S. Wacharasindhu, P. Phuwapraisirisan, *N*-arylmethylaminoquercitols, a new series of effective antidiabetic agents having α-glucosidase inhibition and antioxidant activity, Bioorg. Med. Chem. Lett. 25 (2015) 2570–2573.
[9] W. Worawalai, P. Khongchai, N. Surachaitanawat, P. Phuwapraisirisan, Synthesis of furofuran lignans as antidiabetic agents simultaneously achieved by inhibiting α-glucosidase and free radical, Arch. Pharm. Res. 39 (2016) 1370–1381.
[10] W. Worawalai, P. Phuwapraisirisan, Samin-derived flavonolignans, a new series of antidiabetic agents having dual inhibition against α-glucosidase and free radicals, Nat. Prod. Res. (2018), https://doi.org/10.1080/14786419.2018.1553169 inpress.
[11] M. Nakai, M. Harada, K. Nakahara, K. Akimoto, H. Shibata, W. Miki, Y. Kiso, Novel antioxidative metabolites in rat liver with ingested sesamin, J. Agric. Food Chem. 51 (2003) 1666–1670.
[12] A.A. Moazzami, R.E. Andersson, A. Kamal-Eldin, Quantitative NMR analysis of a sesamin catechol metabolite in human urine, J. Nutr. 137 (2007) 940–944.
[13] H. Urata, Y. Nishioka, T. Tobashi, Y. Matsumura, N. Tomimori, Y. Ono, Y. Kiso, S. Wada, First chemical synthesis of antioxidative metabolites of sesamin, Chem. Pharm. Bull. 56 (2008) 1611–1612.
[14] Y.Q. Ye, H. Koshino, J.I. Onose, K. Yoshikawa, N. Abe, S. Takahashi, First total synthesis of vialinin A, a novel and extremely potent inhibitor of TNF-α production, Org. Lett. 9 (2007) 4131–4134.
[15] B.W. Zhang, X. Li, W.L. Sun, Y. Xing, Z.L. Xiu, C.L. Zhuang, Y.S. Dong, Dietary flavonoids and acarbose synergistically inhibit α-glucosidase and lower post-prandial blood glucose, J. Agric. Food Chem. 65 (2017) 8319–8330.
[16] W. Worawalai, P. Sompornpisut, S. Wacharasindhu, P. Phuwapraisirisan, Voglibose-inspired synthesis of new potent α-glucosidase inhibitors *N*-1,3-dihydroxypropylaminocyclitols, Carbohydr. Res. 429 (2016) 155–162.
[17] L. Sim, R. Quezada-Calvillo, E.E. Sterchi, B.L. Nichols, D.R. Rose, Human intestinal maltase-glucoamylase: crystal structure of the N-terminal catalytic subunit and basis of inhibition and substrate specificity, J. Mol. Biol. 375 (2008) 782–792.
[18] V.L. Guilloux, P. Schmidtke, P. Tuffery, Fpocket: an open source platform for ligand pocket detection, BMC Bioinformatics 10 (2009) 168.
[19] M. Tanemura, T. Ogawa, N. Ogita, A new algorithm for three-dimensional voronoi tessellation, J. Comput. Phys. 51 (1983) 191–207.
[20] Z. Zhang, Y. Li, B. Lin, M. Schroeder, B. Huang, Identification of cavities on protein surface using multiple computational approaches for drug binding site prediction, Bioinformatics 27 (2011) 2083–2088.
[21] B.A.H.P.C.B.-H.R. group. Achilles blind docking server, 2017. Available from: < https://bio-hpc.ucam.edu/achilles/ > .
[22] G. Wu, D.H. Robertson, C.L. Brooks 3rd, M. Vieth, Detailed analysis of grid-based molecular docking: a case study of CDOCKER-A CHARMm-based MD docking algorithm, J. Comput. Chem. 24 (2003) 1549–1562.
[23] F.A. Momany, R. Rone, Validation of the general purpose QUANTA 3.2/CHARMm force field, J. Comput. Chem. 13 (1992) 888–900.
[24] J.C. Phillips, R. Braun, W. Wang, J. Gumbart, E. Tajkhorshid, E. Villa, C. Chipot, R.D. Skeel, L. Kale, K. Schulten, Scalable molecular dynamics with NAMD, J. Comput. Chem. 26 (2005) 21.
[25] K. Vanommeslaeghe, E. Hatcher, C. Acharya, S. Kundu, S. Zhong, J. Shim, E. Darian, O. Guvench, P. Lopes, I. Vorobyov, CHARMM general force field: a force field for drug-like molecules compatible with the CHARMM all-atom additive biological force fields, J. Comput. Chem. 31 (2010) 671–690.
[26] K. Vanommeslaeghe, A.D. MacKerell Jr, Automation of the CHARMM general force field (CGenFF) I: bond perception and atom typing, J. Chem. Inf. Model. 52 (2012) 3144–3154.
[27] W. Yu, X. He, K. Vanommeslaeghe, A.D. MacKerell Jr, Extension of the CHARMM general force field to sulfonyl-containing compounds and its utility in biomolecular simulations, J. Comput. Chem. 33 (2012) 2451–2468.
[28] I.S. Gutiérrez, F.-Y. Lin, K. Vanommeslaeghe, J.A. Lemkul, K.A. Armacost, C.L. Brooks III, A.D. MacKerell Jr., Parametrization of halogen bonds in the CHARMM general force field: improved treatment of ligand–protein interactions, Bioorg. Med. Chem. 24 (2016) 4812–4825.
[29] W.L. Jorgensen, J. Chandrasekhar, J.D. Madura, R.W. Impey, M.L. Klein, Comparison of simple potential functions for simulating liquid water, J. Chem. Phys. 79 (1983) 926–935.
[30] T. Darden, D. York, L. Pedersen, Particle mesh Ewald: An N· log (N) method for Ewald sums in large systems, J. Chem. Phys. 98 (1993) 10089–10092.
[31] U. Essmann, L. Perera, M.L. Berkowitz, T. Darden, H. Lee, L.G. Pedersen, A smooth particle mesh Ewald method, J. Chem. Phys. 103 (1995) 8577–8593.
[32] G.J. Martyna, D.J. Tobias, M.L. Klein, Constant pressure molecular dynamics algorithms, J. Chem. Phys. 101 (1994) 4177–4189.